



Targeting of the $\alpha_v\beta_3$ integrin complex by CAR-T cells leads to rapid regression of diffuse intrinsic pontine glioma and glioblastoma

Dustin A Cobb ,¹ Jacopo de Rossi,¹ Lixia Liu,¹ Erin An,¹ Daniel W Lee ^{1,2}

To cite: Cobb DA, de Rossi J, Liu L, *et al.* Targeting of the $\alpha_v\beta_3$ integrin complex by CAR-T cells leads to rapid regression of diffuse intrinsic pontine glioma and glioblastoma. *Journal for ImmunoTherapy of Cancer* 2022;**10**:e003816. doi:10.1136/jitc-2021-003816

► Additional supplemental material is published online only. To view, please visit the journal online (<http://dx.doi.org/10.1136/jitc-2021-003816>).

Accepted 24 January 2022



© Author(s) (or their employer(s)) 2022. Re-use permitted under CC BY-NC. No commercial re-use. See rights and permissions. Published by BMJ.

¹Department of Pediatrics, University of Virginia, Charlottesville, Virginia, USA

²University of Virginia Cancer Center, University of Virginia, Charlottesville, Virginia, USA

Correspondence to

Dr Daniel W Lee;
DWL4Q@virginia.edu

ABSTRACT

Background Diffuse intrinsic pontine glioma (DIPG) and glioblastoma (GBM) are two highly aggressive and generally incurable gliomas with little therapeutic advancements made in the past several decades. Despite immense initial success of chimeric antigen receptor (CAR) T cells for the treatment of leukemia and lymphoma, significant headway into the application of CAR-T cells against solid tumors, including gliomas, is still forthcoming. The integrin complex $\alpha_v\beta_3$ ($\alpha_v\beta_3$) is present on multiple and diverse solid tumor types and tumor vasculature with limited expression throughout most normal tissues, qualifying it as an appealing target for CAR-T cell-mediated immunotherapy.

Methods Patient-derived DIPG and GBM cell lines were evaluated by flow cytometry for surface expression of $\alpha_v\beta_3$. Second-generation CAR-T cells expressing an anti- $\alpha_v\beta_3$ single-chain variable fragment were generated by retroviral transduction containing either a CD28 or 4-1BB costimulatory domain and CD3zeta. CAR-T cells were evaluated by flow cytometry for CAR expression, memory phenotype distribution, and inhibitory receptor profile. DIPG and GBM cell lines were orthotopically implanted into NSG mice via stereotactic injection and monitored with bioluminescent imaging to evaluate $\alpha_v\beta_3$ CAR-T cell-mediated antitumor responses.

Results We found that patient-derived DIPG cells and GBM cell lines express high levels of surface $\alpha_v\beta_3$ by flow cytometry, while $\alpha_v\beta_3$ is minimally expressed on normal tissues by RNA sequencing and protein microarray. The manufactured CAR-T cells consisted of a substantial frequency of favorable early memory cells and a low inhibitory receptor profile. $\alpha_v\beta_3$ CAR-T cells demonstrated efficient, antigen-specific tumor cell killing in both cytotoxicity assays and in *in vivo* models of orthotopically and stereotactically implanted DIPG and GBM tumors into relevant locations in the brain of NSG mice. Tumor responses were rapid and robust with systemic CAR-T cell proliferation and long-lived persistence associated with long-term survival. Following tumor clearance, TCF-1⁺ $\alpha_v\beta_3$ CAR-T cells were detectable, underscoring their ability to persist and undergo self-renewal.

Conclusions These results highlight the potential of $\alpha_v\beta_3$ CAR-T cells for immunotherapeutic treatment of aggressive brain tumors with reduced risk of on-target, off-tumor mediated toxicity due to the restricted nature of $\alpha_v\beta_3$ expression in normal tissues.

BACKGROUND

While chimeric antigen receptor (CAR)-T cells are changing the treatment paradigm for many hematologic cancers,^{1–6} CAR-T cells as a viable therapeutic strategy against solid tumors has been met with challenges resulting in a lack of major advancement. They include heterogeneous expression and downregulation of target antigen, unacceptable levels of antigen expression in normal tissues, impaired CAR-T cell trafficking, and immunosuppressive tumor microenvironments^{7–8}. Common CAR-T cell targets receiving attention include B7-H3, EGFRvIII, GD2, HER2, and mesothelin.^{9–12} Finding additional targets broadly expressed on many tumors but not on normal tissues would greatly advance the field as clinical development of just one therapeutic could be widely applicable to many cancers.

Integrins are heterodimeric adhesion receptors important for cell migration, tissue invasion, and in some cases survival of tumors themselves. Additionally, they are critical for angiogenesis, being expressed on neovascular endothelium feeding growing tumors, and via this role can contribute to tumor progression and metastasis.¹³ Integrin $\alpha_v\beta_3$ ($\alpha_v\beta_3$) expression is typically limited to newly forming endothelial cells^{14–15}; however, its presence has been associated with a number of tumors, particularly within the central nervous system (CNS).^{16–18} Previous studies of $\alpha_v\beta_3$ as a therapy target focused on inhibiting its angiogenic role in tumorigenesis due to its expression on endothelial cells within tumor vasculature. The small molecule, cilengitide, an $\alpha_v\beta_3$ and $\alpha_v\beta_5$ antagonist was safe in phase I/II trials in children and adults with high-grade, $\alpha_v\beta_3$ -expressing gliomas but was not effective.¹⁹ Similarly, antibodies targeting $\alpha_v\beta_3$ did not demonstrate a therapeutic benefit in patients with melanoma, leiomyosarcoma,

and other solid tumors.^{20–23} Despite the lack of efficacy, disrupting $\alpha_v\beta_3$ did not have any significant toxicities, making it attractive as a potential CAR-T cell therapeutic. In addition, since $\alpha_v\beta_3$ is upregulated on non-malignant vascular endothelium feeding tumors,²⁴ $\alpha_v\beta_3$ CAR-T cells may still be effective even if tumors themselves downregulate the target, a frequent phenomenon driving CAR-T cell resistance. To date, no other CAR-T cell has been developed that targets both tumor and surrounding vasculature.

Though $\alpha_v\beta_3$ is known to be expressed on glioblastoma (GBM) and melanoma, studies investigating the breadth of targeting it with CAR-T cells are lacking. Screening additional tumor types for $\alpha_v\beta_3$, correlating functional assays including xenograft models to rigorously test the efficacy and safety of $\alpha_v\beta_3$ CAR-T cells, and deeper analysis of $\alpha_v\beta_3$ CAR-T cell antitumor response characteristics are necessary. In this study, we sought to evaluate the ability of $\alpha_v\beta_3$ CAR-T cells to target the histone H3K27M mutant diffuse midline glioma, diffuse intrinsic pontine glioma (DIPG), and GBM brain tumors, two highly lethal malignancies currently lacking effective therapeutics. DIPG is a highly aggressive tumor of the pons during early childhood and is universally fatal within 1 year on average even with aggressive interventions.^{25,26} Likewise, GBM, the most common primary brain tumor in adults, is characterized by very poor survival and limited effective therapeutics.²⁷ We designed and tested new $\alpha_v\beta_3$ CAR-T cells in separate orthotopic brain tumor xenograft models representing DIPG and GBM. Our results provide a comprehensive evaluation of CAR-T cell products and analyses of the antitumor responses of $\alpha_v\beta_3$ CAR-T cells including efficacy, persistence, and memory cell characteristics in vivo following treatment of these CNS tumors.

MATERIALS AND METHODS

Cell lines

Tumor cell lines were obtained from the following sources: patient-derived DIPG cells were kindly provided by M. Monje (Stanford University), U87 from L. Lum (University of Virginia), and U251 from D. Brautigam (University of Virginia). Maintenance and culture of DIPG lines was performed according to an established protocol.²⁸ U87, U251, and 293GP from C. Mackall (Stanford University) were maintained in DMEM containing 10% FBS. Tumor cells were lentivirally transduced with eGFP/firefly luciferase (eGFP/ffLuc). SU-DIPG-36 and U87 were single-cell cloned and evaluated for GFP by flow cytometry. Peripheral blood mononuclear cells (PBMCs) were obtained from healthy and consenting donors by apheresis under an Institutional Review Board approved protocol (UVA-IRB#18842).

CAR-T cell construct design, synthesis, and cloning

The scFv sequence for targeting $\alpha_v\beta_3$ was derived from the monoclonal antibody clone LM609 with assistance from the University of Virginia Antibody Engineering and

Technology Core. The variable regions of the heavy and light chains were assembled with a (GGGGs₃) linker. The scFv sequence was preceded by the human GM-CSF-R signal sequence and followed by human CD8 α hinge and transmembrane domain. This was linked to either a CD28 or 4-1BB intracellular signaling domain followed by the CD3 ζ signaling chain. The entire construct was generated by gene synthesis (ThermoFisher). CAR constructs were then cloned into a retroviral vector. After sub-cloning, sequences were confirmed by DNA sequencing.

Retrovirus production and T cell transduction

Retroviruses were produced via transient transfection of 293GP cells. Cells were seeded on poly-D-lysine-coated plates (10mg/cm²) and transfected via Lipofectamine2000 (ThermoFisher) with plasmids encoding the CARs and RD114. PBMCs were stimulated with T cell activation and expansion beads (ThermoFisher) at a 1:1 ratio with 40 IU/mL IL-2 for 3 days. Retroviral supernatants were added to Retronectin-coated plates (Takara) and centrifuged for 2 hours. T cells were transduced on days 3 and 4 and cultured in AIM-V medium (ThermoFisher) containing 5% fetal bovine serum (FBS), 1% L-glutamine, 1% HEPES and 1% Pen/Strep with 300 IU/mL IL-2. Beads were removed on day 5, and T cells were expanded with 300 IU/mL IL-2 until harvest.

Flow cytometry

Surface expression of $\alpha_v\beta_3$ on tumor cells was evaluated by staining with PE-conjugated anti- $\alpha_v\beta_3$ (LM609; Millipore Sigma) or isotype control. Analysis of CAR-T cells was performed using antibodies against CD3 (HIT3a), CD4 (OKT4), CD8 (SK1), CD45RO (UCHL1.1), CD45RA (H100), CCR7 (G043H7), CD127 (A019D5), PD-1 (EH12.2H7), LAG-3 (11C3C65), TIM-3 (F38-2E2), CD45 (2D1), and TCF-1 (7F11A10) (Biolegend). Expression of $\alpha_v\beta_3$ CAR was detected using biotinylated protein-L (ThermoFisher) followed by streptavidin-PE (Biolegend). Intracellular staining for TCF-1 was performed using Foxp3/Transcription Factor Staining Buffer Set (eBioscience). All samples were stained with Fixable Viability dye (Biolegend). Data were acquired on a NovoCyte3005 Flow Cytometer (ACEA Biosciences) and analyzed using FlowJo v10.

Cytotoxicity and cytokine production assays

Cytotoxicity was evaluated using a luciferase-based assay measuring bioluminescence. Tumor cells expressing eGFP/ffLuc were cocultured with non-transduced T cells, CD19.28 ζ , $\alpha_v\beta_3$ -28 ζ , or $\alpha_v\beta_3$ -BB ζ CAR-T cells for 18 hours at effector-to-target (E:T) ratios ranging from 10:1 to 2.5:1. Tumor cell lysis was determined by measuring residual luciferase activity and calculated as follows: percent lysis = 100 - (((average signal from T cell treated tumor wells) / (average signal from untreated target tumor wells)) × 100). In vitro cytokine production by CAR-T cells was evaluated through cocultivation of non-transduced T cells, CD19.28 ζ , $\alpha_v\beta_3$ -28 ζ , or $\alpha_v\beta_3$ -BB ζ CAR-T cells

with tumor cells at a 1:1 ratio. Effector cell numbers were normalized across each group with transduction efficiency of CAR⁺ T cells. Coculture supernatants were collected after 24 hours and tested for interferon gamma (IFN- γ), interleukin-2 (IL-2), and tumor necrosis factor alpha (TNF- α) by ELISA (Biolegend).

Orthotopic xenogeneic mouse models

For DIPG, 5×10^5 patient-derived SU-DIPG-36 cells expressing eGFP/fLuc were implanted by stereotactic injection into the pons of 6–8 weeks old NOD-scid IL2Rg⁻ (NSG) mice (coordinates from lambda: M/L: +1mm; A/P: -0.8mm; D/V: -5mm). For GBM, 5×10^5 U87 cells expressing eGFP/fLuc were implanted by stereotactic injection into the pons of NSG mice (coordinates from bregma: M/L: +3mm; A/P: +1mm; D/V: -3.5mm). On day 21, 2×10^6 CAR-T cells were delivered intratumorally using the same coordinates for tumor implantation. Tumor burden was assessed at least weekly via bioluminescent imaging (BLI) following intraperitoneal injection of D-luciferin (IVIS Spectrum; PerkinElmer). Progression-free survival was determined as the number of days from CAR-T cell treatment to the first day of disease progression or death.

Immunohistochemistry

A 20-organ normal tissue microarray (TMA; BN1002b; US BioMax) was stained with anti- $\alpha_v\beta_3$ antibody (23C6; R&D Systems) (performed by the Biorepository and Tissue Research Facility core; University of Virginia). For staining of DIPG tumor cells in mouse brain tissue, mice were perfused and brains harvested and fixed in paraformaldehyde. Brain sections were stained with anti- $\alpha_v\beta_3$ antibody (LM609). Slides were digitally scanned and evaluated for $\alpha_v\beta_3$ staining in QuPath, an open-source software application for digital histopathology analysis.²⁸ Positive cell detection was performed on normal tissue TMA and mouse brain tissues at three threshold levels (1+, 2+, and 3+), and H-scores were calculated by using the following formula: $[1 \times (\% \text{ cells } 1+) + 2 \times (\% \text{ cells } 2+) + 3 \times (\% \text{ cells } 3+)]$.

Statistical analysis

All statistical analyses were performed using GraphPad Prism. Data are presented as means \pm SEM unless otherwise noted in figure legends. Results were analyzed by one-way or two-way analysis of variance (ANOVA) with Tukey's multiple comparisons post-test or unpaired non-parametric Mann-Whitney test for determining significant differences between experimental groups. Kaplan-Meier survival analysis was performed with Log-rank (Mantel-Cox) test for comparison between treatment groups. Bioluminescence images and data were analyzed with Living Image Software (PerkinElmer). Analysis of tumor growth curves was performed by first transforming bioluminescent values of individual mice at each time point to log form and then confirming Gaussian distribution using the Shapiro-Wilk test for normality. Unless

noted in figure legends, means of each treatment group were compared at each time point by two-way ANOVA with Tukey's multiple comparisons post-test.

RESULTS

$\alpha_v\beta_3$ expression on DIPG, GBM and normal tissues

Given that $\alpha_v\beta_3$ expression has been reported across some cancers, we sought to evaluate expression on DIPG and GBM for the purpose of CAR-T cell-directed therapy. $\alpha_v\beta_3$ expression was detected on 6/6 patient-derived DIPG lines and 2/2 GBM lines screened (figure 1A). In particular, $\alpha_v\beta_3$ was highly expressed on SU-DIPG-36, SU-DIPG-IV, SU-DIPG-21 (H3.1K27M mutants) and exhibited moderate expression on SU-DIPG-13, SU-DIPG-17, and SU-DIPG-27 (H3.3K27M mutants) (figure 1B). $\alpha_v\beta_3$ was also highly expressed on GBM (U87 and U251). The cancer cell lines H358 (lung), BT-20 (breast), and Caco-2 (colon) were negative for $\alpha_v\beta_3$ expression. These data are supported by publicly available gene expression data in DIPG and pediatric GBM patient specimens, particularly for integrin α_v (*ITGAV*), relative to normal tissues (online supplemental figure 1A). Additionally, we found within the Cancer Cell Line Encyclopedia project database that glioma cell lines as a whole were elevated in expression of *ITGAV* and *ITGB3* relative to other lines (including B-ALL, T-ALL, AML, and neuroblastomas) and normal organ tissues (online supplemental figure 1B). These results support the potential for CAR-T cell-directed targeting in this setting.

Given the high-level of CAR-T cell activity in patients following antigen exposure, limiting 'on-target, off-tumor' toxicities due to normal tissue expression of antigen is imperative for safe clinical usage. While $\alpha_v\beta_3$ expression is well characterized and has been shown to be primarily restricted to endothelial cells in newly forming blood vessels and absent in resting endothelial cells in normal organ systems, we performed additional screening for its presence in normal tissues. First, we performed gene expression analysis of *ITGAV* and *ITGB3* using the expO Normal Tissue Expression array in the NCI Oncogenomics Database. Neither gene was highly expressed in represented normal organ tissues, except *ITGB3* in the thyroid (figure 1C). Second, we assessed expression of $\alpha_v\beta_3$ by immunohistochemistry in a normal human tissue microarray consisting of 20 organ types, each from five individual donors (figure 1D). $\alpha_v\beta_3$ staining was absent in nearly all or exhibited minimal staining in others as determined by H-score (figure 1E). Of note, skin (3/5 donors) and ovary (2/4 donors) exhibited detectable but modest staining. These results provide further validation of the limited expression of $\alpha_v\beta_3$ in normal healthy tissues, supporting the targeting of this integrin by CAR-T cells.

Design and phenotypic characterization of CAR-T cells redirected against $\alpha_v\beta_3$

The scFv domain used in the design of the CARs targeting $\alpha_v\beta_3$ was based on the well-characterized monoclonal

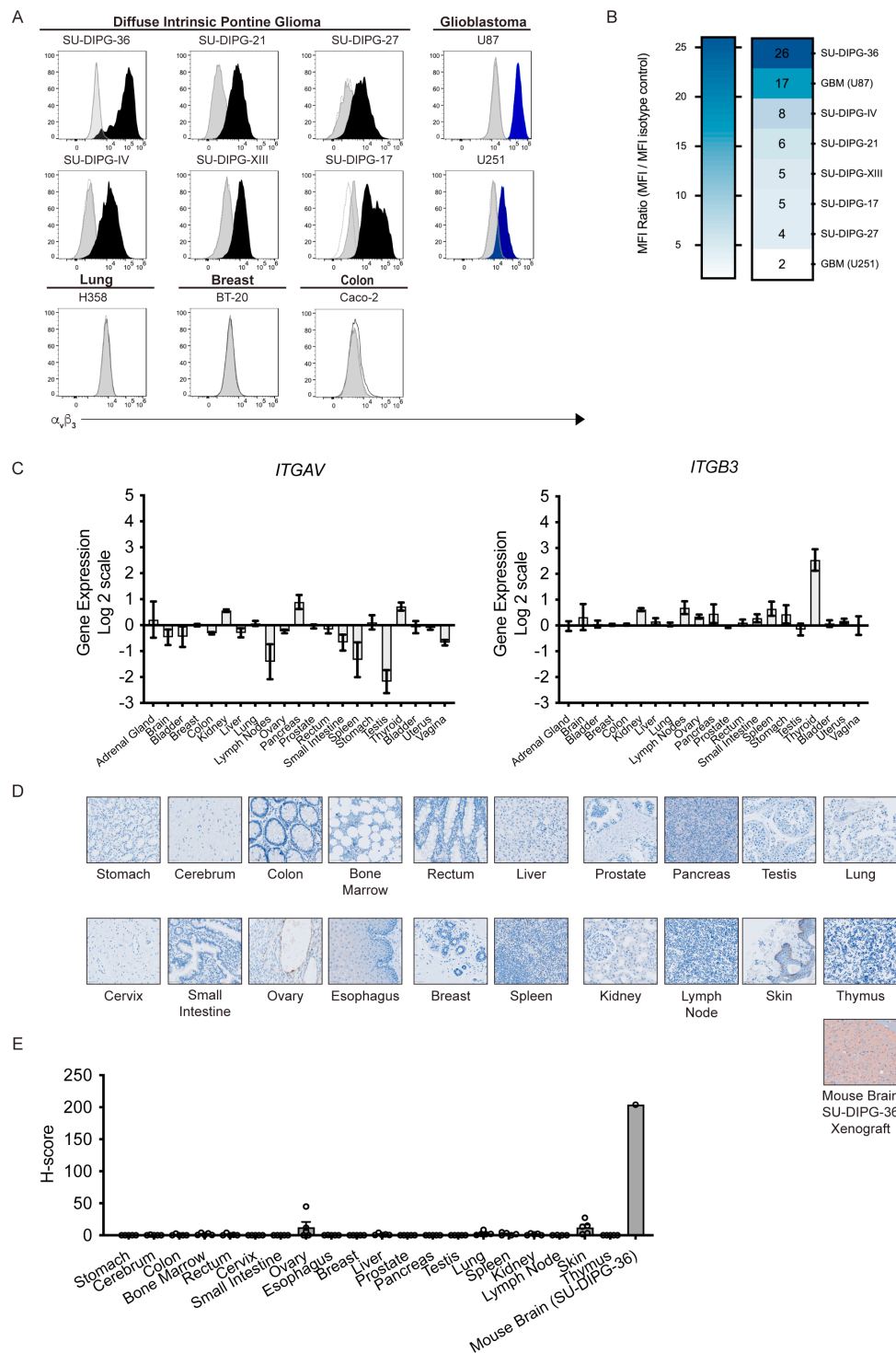


Figure 1 The integrin complex $\alpha_v\beta_3$ is highly expressed on patient-derived DIPG cells and GBM tumor cell lines. (A) Representative histograms from flow cytometry analysis of DIPG, GBM, lung (H358), breast (BT-20), and colon (Caco-2) tumor cell lines surface stained with anti- $\alpha_v\beta_3$. Gray dotted line histograms indicate unstained tumor cells, gray-shaded histograms represent staining with an isotype control antibody, and solid color-filled histograms indicate tumor cells stained with anti- $\alpha_v\beta_3$ antibody (clone LM609). (B) Heat map summarizing the expression of $\alpha_v\beta_3$ across multiple DIPG and GBM tumor cell lines. The MFI ratio (MFI/MFI isotype control) for $\alpha_v\beta_3$ in each cell type was calculated and ranked from highest to lowest. (C) Gene expression for *ITGAV* and *ITGB3* within normal human tissues obtained by accessing Affymetrix mRNA expression data within the expO Normal Tissue Expression microarray via the NIH Pediatric Oncology Branch Oncogenomics Database. (D) Immunohistochemical staining for $\alpha_v\beta_3$ expression was performed on a normal human TMA containing 20 different tissue types from five different donors and brain tissue from a mouse with a human DIPG xenograft (SU-DIPG-36). Shown are representative tissue cores from each tissue type. (E) $\alpha_v\beta_3$ normal tissue expression was quantified by H-score for each tissue type and is represented in the bar graph. Data are shown as mean \pm SEM. $\alpha_v\beta_3$, $\alpha_v\beta_3$; DIPG, diffuse intrinsic pontine glioma; GBM, glioblastoma; TMA, tissue microarray.

antibody clone LM609. LM609 has been previously evaluated in various clinical studies and found to be safe but with no reported treatment efficacy.^{23–29} For the purposes of our study, we designed two $\alpha_v\beta_3$ -CAR constructs with humanized and optimized LM609 V_H and V_L chains, followed by the CD8 α transmembrane domain, and CD28 or 4-1BB costimulation with CD3 ζ (figure 2A). $\alpha_v\beta_3$,28 ζ and $\alpha_v\beta_3$,BB ζ CARs were highly expressed by T cells, exhibiting an average of 76% and 66% positivity, respectively, across multiple normal donors (figure 2B). Positivity and surface expression levels (eg, MFI) of $\alpha_v\beta_3$,28 ζ and $\alpha_v\beta_3$,BB ζ CARs were comparable to the CD19,28 ζ CAR,^{30–31} which was included throughout this study as a negative control and for comparison purposes. $\alpha_v\beta_3$ CAR-T cells exhibited vigorous ex vivo expansion ranging from 100 to 1000-fold by day 7–9 post-transduction (figure 2C).

Successful clinical outcomes from CAR-T cell therapy occur when cell persistence and memory formation are achieved. Specifically, less-differentiated CAR-T cells and memory populations have been shown to exhibit superior antitumor responses.³² Therefore, we assessed the memory cell populations of $\alpha_v\beta_3$ CAR-T cells following ex vivo expansion. Evaluation by flow cytometry revealed a spectrum of memory and effector subset differentiation. Expanded $\alpha_v\beta_3$ CAR-T cells were comprised of effector and central memory subsets as well as stem cell memory T-like cells (figure 2D). There were no significant differences in the overall percentage of CD45RO⁺ populations in CD4⁺ T cells between non-transduced T cells, $\alpha_v\beta_3$,28 ζ , $\alpha_v\beta_3$,BB ζ , or CD19,28 ζ CAR-T cells; however, CD8⁺ T cells exhibited increased frequencies of CD45RO⁺ cells in $\alpha_v\beta_3$,28 ζ and $\alpha_v\beta_3$,BB ζ CAR-T cells relative to controls (figure 2E). Both CD8 and CD4 $\alpha_v\beta_3$,BB ζ CAR-T cell populations trend towards a less differentiated profile compared with $\alpha_v\beta_3$,28 ζ CAR-T cells, although, there were no statistically significant differences between the two among profiled subsets except in the frequency of CD8⁺CCR7⁺CD127⁺ effector memory cells (figure 2F). The modest differences in CAR-T cell differentiation may be attributed to some form of low-level activation as a result of CAR expression.

$\alpha_v\beta_3$ CAR-T cells efficiently eliminate DIPG and GBM in vitro

The antitumor activity of $\alpha_v\beta_3$ CAR-T cells was evaluated by determining cytotoxicity and effector cytokine production against DIPG and GBM tumor cells in vitro. CAR-T cell-mediated cytotoxicity was evaluated against patient-derived DIPG lines, SU-DIPG-36, SU-DIPG-XIII, SU-DIPG-IV, and SU-DIPG-17 by exposing eGFP/ffLuc-expressing DIPG cells to non-transduced, CD19,28 ζ , $\alpha_v\beta_3$,28 ζ , or $\alpha_v\beta_3$,BB ζ CAR-T cells at E:T ratios ranging from 10:1 to 2.5:1. Both $\alpha_v\beta_3$ CAR-T cells exhibited substantial tumor cell killing against each DIPG line at all E:T ratios, with $\alpha_v\beta_3$,BB ζ CAR-T cells showing a more modest yet still high level of killing at the lowest E:T ratio (figure 3A,B). Little to no cytotoxicity of DIPG cells was observed when cocultured with non-transduced or CD19 CAR-T cells. DIPG tumor cells also induced significant

levels of effector cytokine production by $\alpha_v\beta_3$ CAR-T cells, but not controls, as determined by measurements of secreted IFN- γ , IL-2, and TNF- α (figure 3C). These data show the specific and robust antitumor responses of $\alpha_v\beta_3$ CAR-T cells against DIPG. Next, we evaluated efficacy of $\alpha_v\beta_3$ CAR-T cells against GBM. Antitumor activity of $\alpha_v\beta_3$ CAR-T cells was evaluated against eGFP/ffLuc-expressing U87 and U251. Both $\alpha_v\beta_3$,28 ζ and $\alpha_v\beta_3$,BB ζ CAR-T cells exhibited a high degree of tumor cell killing at all E:T ratios (figure 3D,E). Furthermore, $\alpha_v\beta_3$ CAR-T cells produced effector cytokines on GBM tumor cell exposure (figure 3F). The $\alpha_v\beta_3$ -negative cell lines H358 and BT-20 (figure 1A) were used as target cells to validate specificity of antitumor activity against $\alpha_v\beta_3$. Importantly, there was an absence of cytotoxicity of $\alpha_v\beta_3$,28 ζ and $\alpha_v\beta_3$,BB ζ CAR-T cells against BT-20 and H358 (figure 3G), indicating that expression of $\alpha_v\beta_3$ on target cells is necessary for antitumor activity. Lastly, $\alpha_v\beta_3$,28 ζ and $\alpha_v\beta_3$,BB ζ CAR-T cell killing of U87 tumor cells was abolished following target blockade via anti- $\alpha_v\beta_3$ antibody (LM609), demonstrating specificity of the CAR for $\alpha_v\beta_3$ (figure 3H). These results demonstrate that $\alpha_v\beta_3$,28 ζ and $\alpha_v\beta_3$,BB ζ CAR-T cells are highly effective at killing DIPG and GBM brain tumor cells expressing $\alpha_v\beta_3$.

$\alpha_v\beta_3$ CAR-T cells induce rapid tumor regression of well-established orthotopic DIPG tumors

In order to validate antitumor activity of $\alpha_v\beta_3$ CAR-T cells and to demonstrate in vivo efficacy, we used an orthotopic xenograft model for DIPG. First, NOD-*scid*-IL2R γ ^{null} (NSG) mice were implanted with SU-DIPG-36 cells expressing GFP/ffLuc into the pons region of the brainstem using previously established stereotactic coordinates^{33–34} (figure 4A). Tumor cell engraftment within the pons was confirmed by H&E staining and immunohistochemical staining for human $\alpha_v\beta_3$ (figure 4B). At 3 weeks postimplantation, pretreatment tumor burden was assessed using bioluminescent imaging indicating that DIPG tumors were large and well established. Tumor-bearing mice were then administered 2×10^6 control CD19,28 ζ , $\alpha_v\beta_3$,28 ζ , or $\alpha_v\beta_3$,BB ζ CAR-T cells by intratumoral (IT) injection using the same coordinates as tumor implantation.

In three independent experiments, using CAR-T cells generated from three different normal human donors, we observed rapid tumor regression within the first week of treatment in mice administered $\alpha_v\beta_3$ CAR-T cells (figure 4C,D). In contrast, tumors in mice receiving CD19,28 ζ CAR-T cells continued to progressively grow. By day 14 post-treatment, tumors in $\alpha_v\beta_3$,28 ζ CAR-T cell treated mice were reduced to background bioluminescent levels. Similarly, tumors in mice treated with $\alpha_v\beta_3$,BB ζ CAR-T cells were also significantly reduced, but remained detectable. Tumors did eventually recur; however, longitudinal monitoring showed that $\alpha_v\beta_3$ CAR-T cells slowed or partially inhibited DIPG growth for an extended period of time as evidenced by the length of progression-free survival (figure 4E). Of note, tumor recurrence in

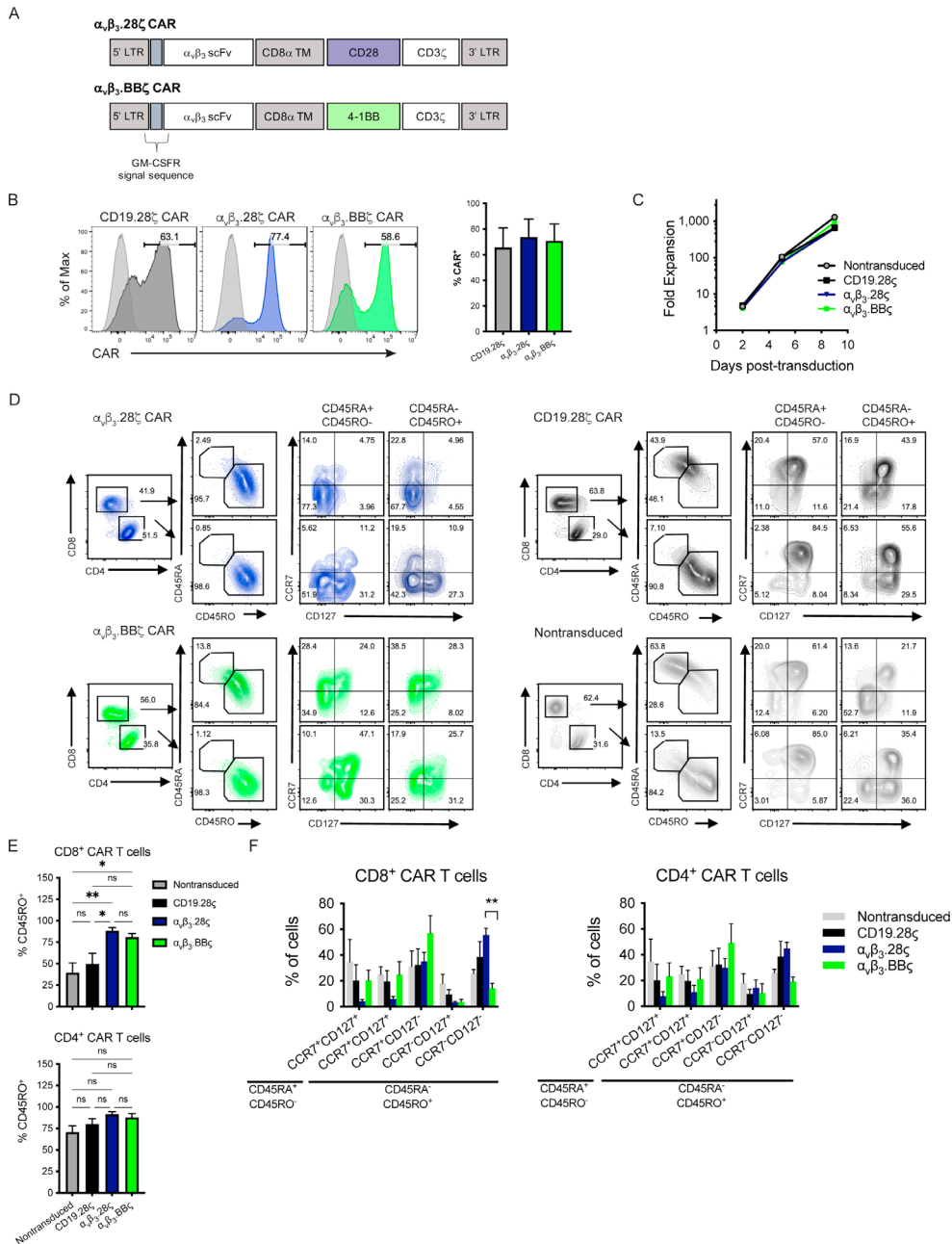


Figure 2 Design, production, and immunophenotypic characterization of $\alpha_v\beta_3$ CAR-T cells following retroviral transduction and ex vivo expansion. (A) Schematic representation of the $\alpha_v\beta_3$ CAR constructs. The anti- $\alpha_v\beta_3$ scFv targeting domain derived from the monoclonal antibody LM609 is preceded by the signal peptide for granulocyte-macrophage colony stimulating factor receptor (GM-CSFR). Following the scFv is the CD8 α transmembrane domain, either CD28 or 4-1BB intracellular signaling domain and CD3 ζ . (B) Left: representative histograms of CAR surface expression gated on CD3⁺ T cells. CAR expression was detected with biotinylated protein L followed by streptavidin-PE and analyzed by flow cytometry. Numbers on histograms represent the percentage of CAR positive cells. Right: bar graph shows the mean transduction efficiency of CD3⁺ T cells on days 9–10 post-transduction from 11 independent CAR-T cell productions using PBMCs from three different normal donors. (C) Representative experiment showing fold expansion of CAR-T cells after retroviral transduction. (D) Flow cytometry gating strategy for identification and evaluation of memory cell differentiation including ‘TSCM-like’ memory (CD45RA⁺CD45RO⁻CCR7⁺CD127⁺), central memory (CD45RO⁻CCR7⁺CD127⁺), and effector memory populations (CD45RO⁺CCR7⁻CD127⁻). Shown are representative contour plots for $\alpha_v\beta_3$ 28 ζ CAR-T cells (top left/blue), $\alpha_v\beta_3$ BB ζ CAR-T cells (bottom left/green), CD19.28 ζ CAR-T cells (top right/black), and non-transduced T cells (bottom right/gray). (E) Percentage of CAR-T cells that are CD45RO⁺ in CD8⁺ and CD4⁺ T cell subsets. (F) Graphical representation of the frequencies of CD8⁺ and CD4⁺ memory T cell subsets following CAR-T cell expansion protocol. (D–F) Characterization of memory subsets were performed on CAR-T cells generated from three different normal donors and results shown are from four independent experiments. *P<0.05 and **p<0.01 were determined by one-way ANOVA (in E) or two-way ANOVA (in F). Data are shown as mean±SEM. $\alpha_v\beta_3$, alpha_v beta₃; ANOVA, analysis of variance; CAR, chimeric antigen receptor; scFv, single-chain variable fragment

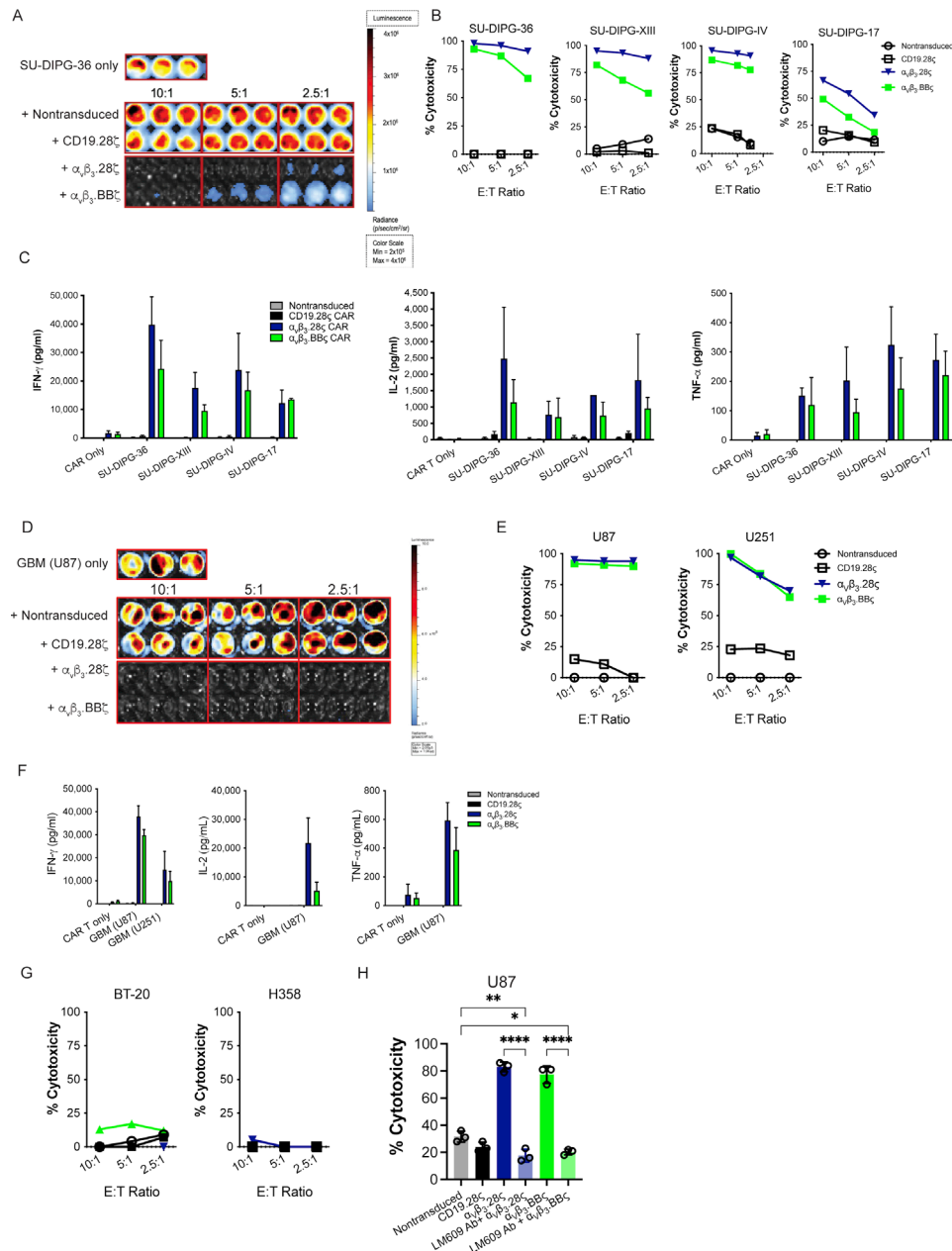


Figure 3 In vitro antitumor activity of $\alpha_v\beta_3$ CAR-T cells against DIPG and GBM. (A) In an 18-hour bioluminescence-based cytotoxicity assay, DIPG tumor cells were cocultured with non-transduced T cells, CD19.28 ζ CAR, $\alpha_v\beta_3$.28 ζ CAR, or $\alpha_v\beta_3$.BB ζ CAR-T cells at E:T ratios ranging from 10:1 to 2.5:1. Bioluminescence of viable tumor cells (luciferase activity) was measured within 20 min following addition of D-luciferin. A representative image capturing bioluminescence is shown. Coculture groups were plated in triplicate wells. (B) Percent cytotoxicity of CAR-T cells against SU-DIPG-IV, SU-DIPG-XIII, SU-DIPG-36, and SU-DIPG-XVII. (C) Effector cytokine production by CAR-T cells was measured in DIPG tumor cell cocultures after 24 hours. Levels of IFN- γ (left), IL-2 (middle), and TNF- α (right) were measured by ELISA. Bar graphs represent the mean cytokine values from multiple donors in at least two to three independent experiments. (D) GBM tumor cells were cocultured with non-transduced T cells, CD19.28 ζ CAR, $\alpha_v\beta_3$.28 ζ CAR, or $\alpha_v\beta_3$.BB ζ CAR-T cells at E:T ratios ranging from 10:1 to 2.5:1. (E) Percent cytotoxicity of CAR-T cells against GBM U87 and U251 cell lines. (F) Effector cytokine production by CAR-T cells was measured in GBM U87 tumor cell cocultures after 24 hours. Levels of IFN- γ (left), IL-2 (middle), and TNF- α (right) were measured by ELISA. Bar graphs represent the mean cytokine values from multiple donors in at least three to four independent experiments. (G) Percent cytotoxicity of CAR-T cells against $\alpha_v\beta_3$ -negative tumor cell lines H358 and BT-20. (H) For blockade of $\alpha_v\beta_3$ -specific cytotoxicity, U87 tumor cells were first incubated with LM609 antibody (10 μ g/mL) for 3 hours, and then cocultured with non-transduced T cells, CD19.28 ζ CAR, $\alpha_v\beta_3$.28 ζ CAR, or $\alpha_v\beta_3$.BB ζ CAR-T cells at an E:T ratio of 2.5:1 in triplicate wells for each group. Tumor cell bioluminescence was then measured following overnight incubation. Data in the bar graph show a representative experiment that was performed twice. (B and E) Experiments were performed at least three times. (C and F) Experiments for each tumor line were performed two to three times with CARs generated from different donors and data are shown as mean \pm SEM. (H) * P <0.05, ** p <0.01, **** p <0.0001 were determined by one-way ANOVA. Data in bar graph are shown as mean \pm SD. ANOVA, analysis of variance; CARs, chimeric antigen receptors; DIPG, diffuse intrinsic pontine glioma; E:T, effector-to-target; GBM, glioblastoma.

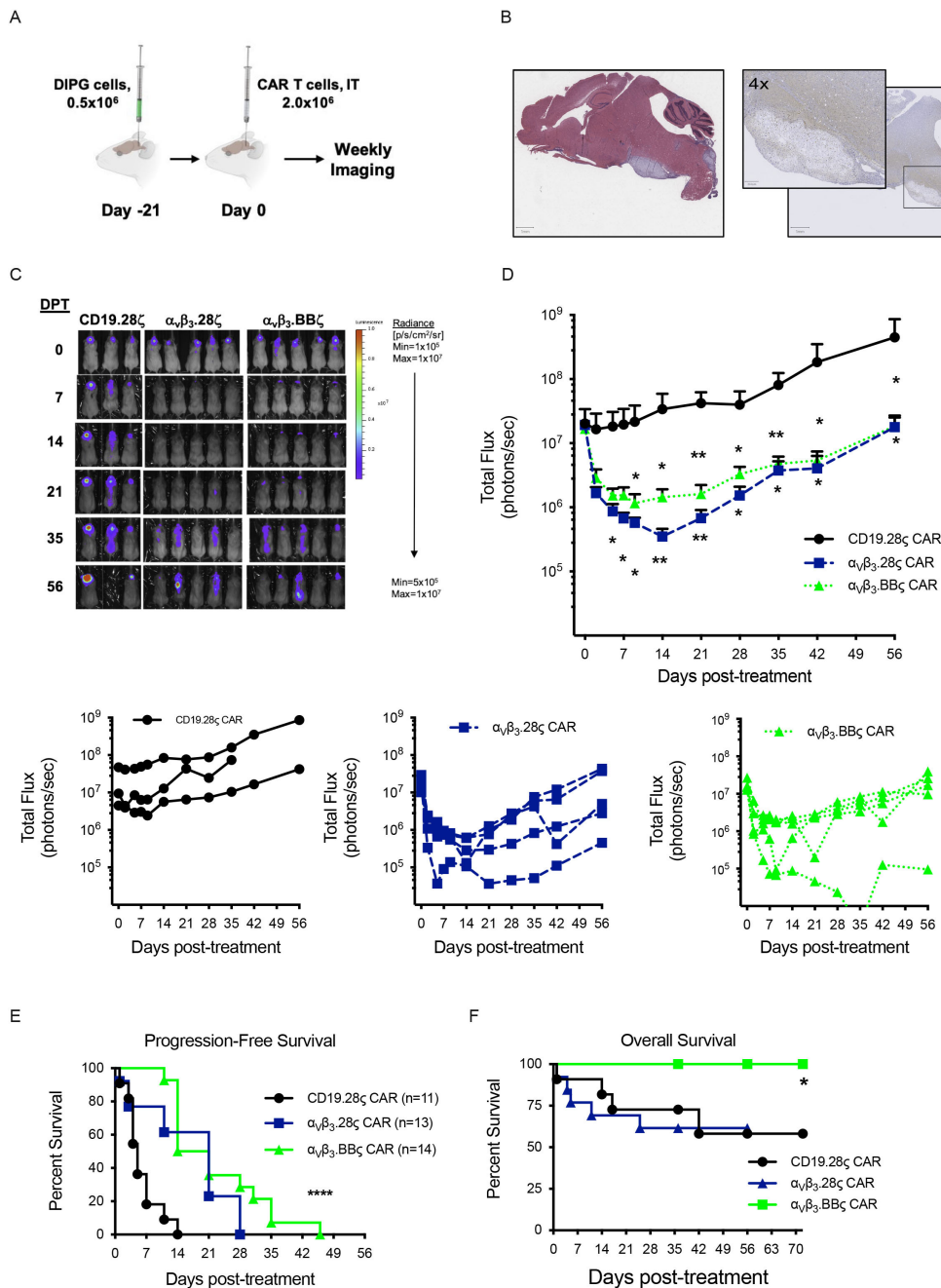


Figure 4 CAR-T cells targeting $\alpha_v\beta_3$ mediate rapid regression of well-established DIPG tumors and limit growth in vivo. (A) Schematic representation of orthotopic DIPG xenograft model. NSG mice implanted with 5×10^5 SU-DIPG-36 (eGFP⁺/ffLuc⁺) were treated intratumorally with 2×10^6 CD19.28 ζ CAR, $\alpha_v\beta_3$.28 ζ CAR, or $\alpha_v\beta_3$.BB ζ CAR-T cells on day 21 postimplantation. (B) H&E (left) and immunohistochemical staining for human $\alpha_v\beta_3$ (right) of a longitudinal brain section from NSG mouse depicting anatomical location of SU-DIPG-36 implantation following stereotactic injection and engraftment. (C) Tumor bioluminescence was measured two to three times per week during the first 2 weeks after CAR-T cell administration and once per week thereafter for the duration of the experiment. Representative experiment showing tumor bioluminescence in DIPG engrafted mice following treatment with CD19.28 ζ CAR (n=3), $\alpha_v\beta_3$.28 ζ CAR (n=5), or $\alpha_v\beta_3$.BB ζ CAR-T cells (n=5). (D) Graphs represent the total flux (photons/second) of tumor bioluminescence in mice treated with CD19.28 ζ CAR, $\alpha_v\beta_3$.28 ζ CAR, or $\alpha_v\beta_3$.BB ζ CAR-T cells in the representative experiment shown in C. Mean values for each treatment group (top) or individual mice in each group (bottom) are shown. (E) Progression-free survival analysis of mice bearing DIPG tumors following CAR-T cell treatment. Progression-free survival was defined as the number of days from CAR-T cell treatment to the first day of disease progression or death. (F) Overall survival analysis of mice following CAR-T cell treatment. (E–F) Results from three independent experiments were pooled (CD19.28 ζ , n=11; $\alpha_v\beta_3$.28 ζ , n=13; $\alpha_v\beta_3$.BB ζ , n=14), and Kaplan-Meier survival analysis was performed with log-rank (Mantel-Cox) test for comparison between treatment groups. The representative experiment shown in figure parts C and D was repeated for a total of three independent experiments. Data are presented as means with error bars representing SEM. P values *p<0.05, **p<0.01, ****p<0.0001 were determined by two-way ANOVA with Tukey's multiple comparisons test. ANOVA, analysis of variance; CAR, chimeric antigen receptor; DIPG, diffuse intrinsic pontine glioma.

CAR-treated mice was slow over time and remained at or below initial pretreatment levels for the duration of the experiment (8 weeks post-treatment). Mice surviving long term required euthanasia due to development of xenogeneic graft-versus-host disease, so additional survival and tumor monitoring could not be completed.

Across three separate and individual experiment replicates, disease resulted in lethality in 42% of mice given CD19 CAR-T cells, whereas 100% of mice that received $\alpha_{\nu}\beta_3$.BB ζ CAR-T cells survived the duration of the experiment (figure 4F). Unexpectedly, 39% of mice that were treated with $\alpha_{\nu}\beta_3$.28 ζ CAR-T cells died, of which most occurred within the first 11 days after injection and following significant reductions in tumor size. This could potentially be due to treatment-induced toxicity and/or trauma associated with repeat injections into the brainstem area. In summary, these results demonstrate that $\alpha_{\nu}\beta_3$ CAR-T cells can act rapidly to significantly reduce DIPG tumors in mice, prolong tumor growth on relapse, and extend survival.

No evidence of T cell exhaustion or antigen escape leading to DIPG recurrence

Tumor recurrence following CAR-T cell treatment can be attributed to various factors including inefficient T cell dose or expansion, exhaustion, lack of CAR-T cell persistence or loss of target antigen expression on tumor cells. In order to determine why DIPG tumors slowly recurred over time following an initial response to $\alpha_{\nu}\beta_3$ CAR-T cell treatment, we investigated whether any of these factors may have contributed to relapse. As expected, reduction in tumor burden coincided with a significant expansion of $\alpha_{\nu}\beta_3$.28 ζ and $\alpha_{\nu}\beta_3$.BB ζ CAR-T cells within the circulation compared with CD19 CAR-T cells by day 14 as these cells were easily detectable following IT administration (figure 5A).

Previous studies have demonstrated that CAR-T cells can become exhausted during ex vivo manufacturing as in the case of GD2.28 ζ CAR-T cells, despite strong in vitro cytotoxicity.³⁵ Thus, expression profiles for the inhibitory receptors PD-1, LAG-3, and TIM-3 on $\alpha_{\nu}\beta_3$.28 ζ and $\alpha_{\nu}\beta_3$.BB ζ CAR-T cells following ex vivo expansion were analyzed (figure 5B). Although $\alpha_{\nu}\beta_3$.28 ζ CAR-T cells did exhibit significantly higher LAG-3 expression on CD8 T cells, inhibitory receptor expression on $\alpha_{\nu}\beta_3$ CAR-T cells was generally comparable with CD19.28 ζ CARs in both CD4 and CD8 T cells (figure 5C). Thus, $\alpha_{\nu}\beta_3$.28 ζ and $\alpha_{\nu}\beta_3$.BB ζ CAR-T cells exhibit inhibitory receptor expression that would be expected as a result of recent T cell activation and are not elevated relative to CD19.28 ζ CAR-T cells following ex vivo production. Given these results, in addition to efficient proliferation during ex vivo expansion (figure 2C), we conclude that $\alpha_{\nu}\beta_3$ CAR-T cells are not exhausted prior to administration into mice bearing DIPG tumors.

To assess the impact of antigen exposure on $\alpha_{\nu}\beta_3$ CAR-T cells in vivo, inhibitory receptor expression was analyzed on CAR-T cells in blood on day 7 and day 14 post-treatment.

PD-1 levels increased slightly from day 7 to day 14 in both $\alpha_{\nu}\beta_3$ CAR groups (figure 5D). LAG-3 and TIM-3 expression levels were low and did not increase from day 7 to day 14 on either CAR-T cell group (figure 5E,F). Importantly, expression levels of PD-1, LAG-3, and TIM-3 on peripheral CAR-T cells were substantially lower relative to their expression induced during initial activation and expansion prior to being transferred into DIPG xenografts. In conclusion, $\alpha_{\nu}\beta_3$ CAR-T cells responding to DIPG tumors in vivo do not appear to show signs of exhaustion at the time when tumors began to regrow, as there was not an overt nor widespread increase in multiple inhibitory receptors, a characteristic indication of the development of T cell exhaustion.^{36 37}

Tumor escape through target antigen loss could have been a cause for DIPG recurrence following $\alpha_{\nu}\beta_3$ CAR-T cell treatment. To address this possibility, brains were harvested at the experimental end-point (day 56), processed for microscopic analysis, and human $\alpha_{\nu}\beta_3$ expression evaluated by immunohistochemistry. $\alpha_{\nu}\beta_3$ expression was detected throughout multiple areas of brain sections indicating significant DIPG tumor infiltration in mice treated with CD19 CAR-T cells. Importantly, strong $\alpha_{\nu}\beta_3$ expression in the pons and subventricular zone from mice treated with either $\alpha_{\nu}\beta_3$ CAR demonstrates that DIPG tumors retain $\alpha_{\nu}\beta_3$ expression following CAR treatment (figure 5G,H). Although $\alpha_{\nu}\beta_3$ expression was detectable in the subventricular zone, a common area of invasion by DIPG,³⁸ tumor infiltration into this region was substantially diminished in $\alpha_{\nu}\beta_3$ CAR-T cell treated mice. Given that $\alpha_{\nu}\beta_3$ expression is retained, these results demonstrate that tumor recurrence following $\alpha_{\nu}\beta_3$ CAR-T cell treatment is not due to target antigen loss.

$\alpha_{\nu}\beta_3$ CAR-T cells eradicate established glioblastoma tumors in mice

To test the in vivo antitumor activity of $\alpha_{\nu}\beta_3$ CAR-T cells against GBM, luciferase-expressing U87 tumor cells were orthotopically implanted into the right forebrain of NSG mice via stereotactic injection, and tumors were allowed to grow for 3 weeks. GBM tumor-bearing mice were administered 2×10^6 CD19.28 ζ , $\alpha_{\nu}\beta_3$.28 ζ , or $\alpha_{\nu}\beta_3$.BB ζ CAR-T cells by IT injection using the same coordinates as tumor implantation. Reduction in tumor burden was evident by day 7 post-treatment in both $\alpha_{\nu}\beta_3$ but not CD19 CAR groups and progressively declined until it was completely eliminated by day 21 (figure 6A,B, online supplemental figure 3A). Not surprisingly, CD28 containing CAR-T cells eliminated tumors more rapidly than 4-1BB CAR-T cells. This is consistent with known effects of CD28 vs 4-1BB signaling on CAR-T cell phenotype, in which CD28 typically provides stronger signaling.^{39 40} Meanwhile, GBM tumors treated with CD19 CAR-T cells continued to grow aggressively.

In contrast to treatment of DIPG tumors, IT treatment of GBM with $\alpha_{\nu}\beta_3$.28 ζ CAR-T cells did not result in any deaths from treatment related toxicity. This suggests that potential toxicity from CAR-T cells may manifest

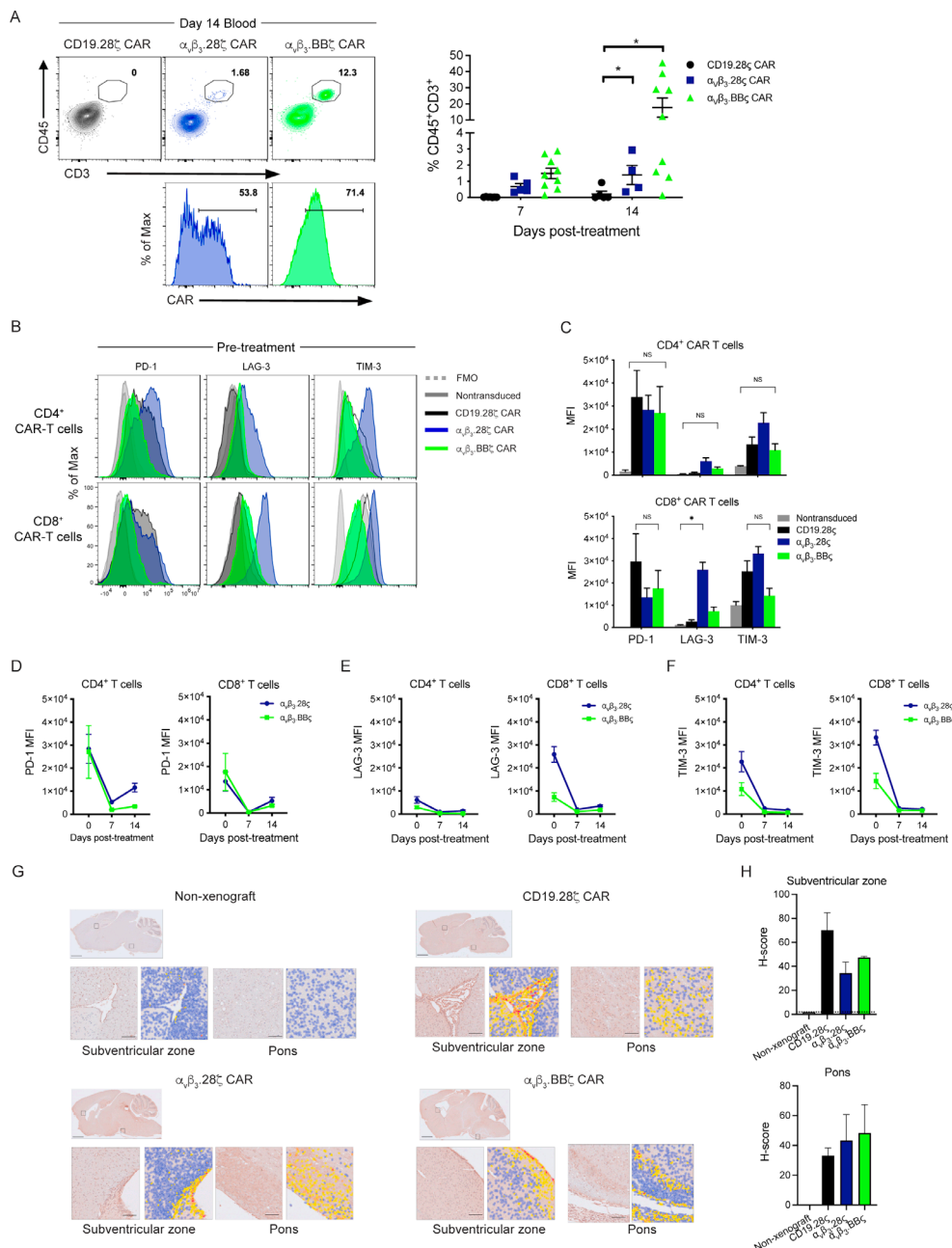


Figure 5 DIPG tumor recurrence in mice treated with $\alpha_v\beta_3$ CAR-T cells does not appear to be a result of poor expansion, T cell exhaustion, or target antigen loss. (A) Peripheral blood was collected on day 7 and day 14 post-treatment for analysis of circulating human T cells ($CD45^+CD3^+$) and CAR expression by flow cytometry. Symbols in graph represent individual mice. (B) CAR-T cells were evaluated for expression of PD-1, LAG-3, and TIM-3 following ex vivo expansion. Representative histograms of PD-1, LAG-3, and TIM-3 expression on $CD4^+$ (top) and $CD8^+$ (bottom) CAR-T cell subsets prior to administration into mice with DIPG xenografts. (C) Graphical representation of the MFI of PD-1, LAG-3, and TIM-3 on $CD4^+$ (top) or $CD8^+$ (bottom) CAR-T cells following ex vivo production and expansion. (D–F) MFI of PD-1, LAG-3, and TIM-3 on $CD8^+$ and $CD4^+$ CAR-T cells (stained with protein L) from peripheral blood of treated mice was analyzed by flow cytometry on day 7 and day 14 post-treatment. (G) Brain tissue sections from SU-DIPG-36 xenografts on day 56 post-treatment with CAR-T cells were evaluated by immunohistochemistry staining for human $\alpha_v\beta_3$. To account for non-specific background staining, non-xenografted mouse brain was used as a control. Scale bars in unmagnified view are 1 mm and bars in insets are 50 μ m. Digital detection overlays over the same fields are shown in adjacent panels. The color scheme is as follows: blue: negative; yellow: low (1+); orange: medium (2+); and red: high (3+). (H) Bar graphs represent the mean H-score values across brain tissue sections from multiple mice ($n=3-4$ /group) treated with CAR-T cells. Non-xenografted brain tissue showed minimal staining, yielding an H-score of 0.08, across the full brain section, 0 in the pons, and 1.9 in the subventricular zone (SVZ) (indicated by dotted line on graph). Data in all graphs are presented as means with error bars representing SEM. * $P<0.05$ was determined by two-way ANOVA with Tukey's multiple comparisons test. (B–C) Characterization of inhibitory receptor profiles was performed on CAR-T cells generated from three different normal donors. ANOVA, analysis of variance; CAR, chimeric antigen receptor; DIPG, diffuse intrinsic pontine glioma.

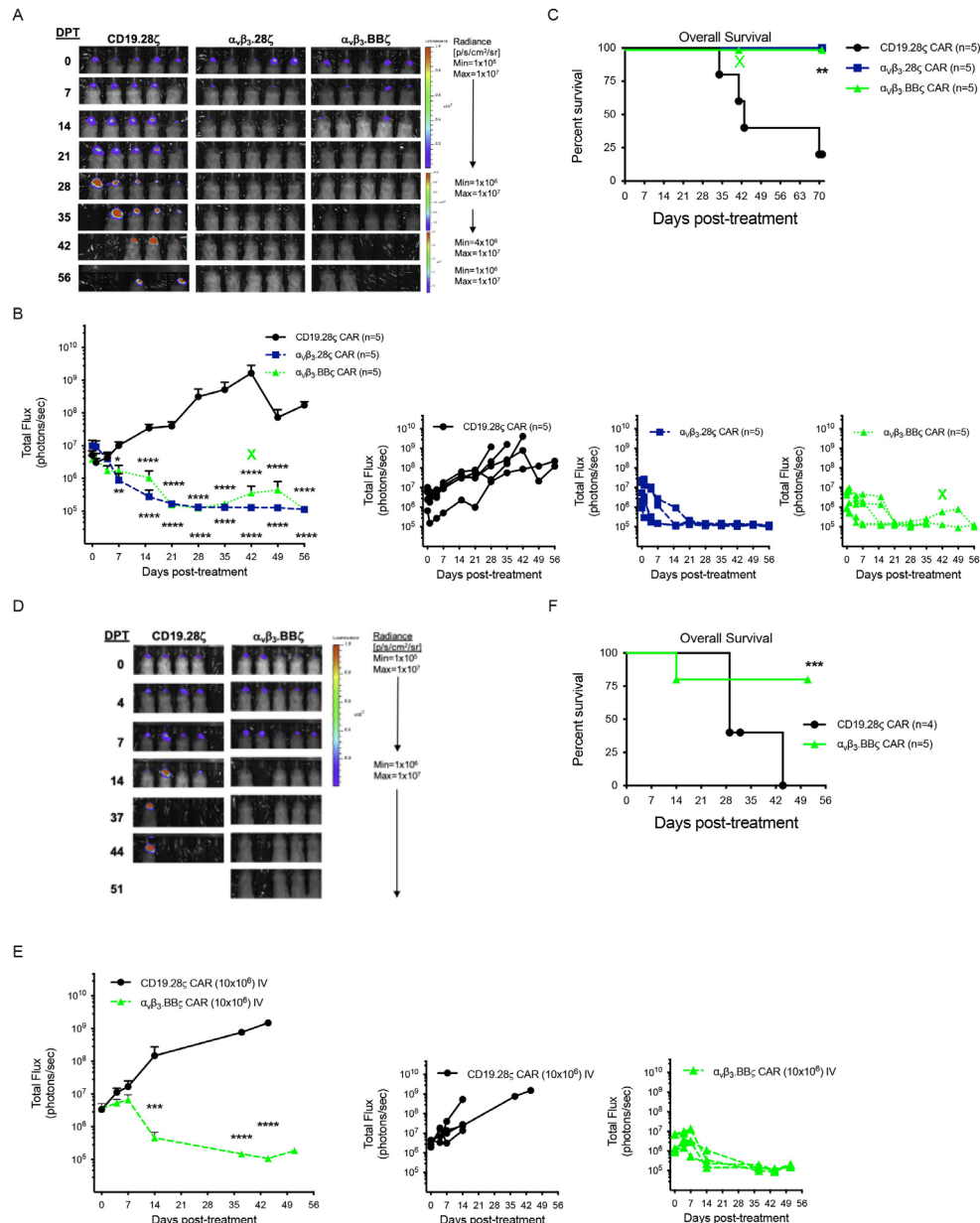


Figure 6 $\alpha_v\beta_3$ CAR-T cells delivered either intratumorally or systemically mediate complete clearance of GBM tumors. (A) NSG mice implanted orthotopically with 5×10^5 GBM (U87) (eGFP⁺/ffLuc⁺) were treated intratumorally with 2×10^6 CD19.28 ζ CAR, $\alpha_v\beta_3.28\zeta$ CAR, or $\alpha_v\beta_3.BB\zeta$ CAR-T cells on day 21 postimplant. Tumor bioluminescence in GBM engrafted mice following treatment with CD19.28 ζ CAR (n=5), $\alpha_v\beta_3.28\zeta$ CAR (n=5), or $\alpha_v\beta_3.BB\zeta$ CAR-T cells (n=5). (B) Graphs represent the total flux (photons/second) of tumor bioluminescence in mice treated with CD19.28 ζ CAR, $\alpha_v\beta_3.28\zeta$ CAR, or $\alpha_v\beta_3.BB\zeta$ CAR-T cells in the representative experiment shown in figure part A. Individual values for each mouse in each group (*left*) or mean values for each treatment group are shown (*right*). (C) Overall survival analysis of mice following CAR-T cell treatment in figure parts A and B. Kaplan-Meier survival analysis was performed with log-rank (Mantel-Cox) test for comparison between treatment groups. (D) NSG mice implanted orthotopically with 5×10^5 GBM (U87) (eGFP⁺/ffLuc⁺) were treated intravenously with 10×10^6 CD19.28 ζ CAR or $\alpha_v\beta_3.BB\zeta$ CAR-T cells on day 21 postimplantation. Representative experiment showing tumor bioluminescence in GBM engrafted mice following treatment with CD19.28 ζ CAR (n=4) or $\alpha_v\beta_3.BB\zeta$ CAR-T cells (n=5). (E) Graphs represent the total flux of tumor bioluminescence in mice treated with CD19.28 ζ CAR or $\alpha_v\beta_3.BB\zeta$ CAR-T cells in the representative experiment shown in figure part D. Individual values for each mouse in each group (*left*) or mean values for each treatment group (*right*) are shown. (F) Overall survival analysis of mice following CAR-T cell treatment in figure parts D and E. Results shown in figure parts A–C (intratumoral CAR-T injection) and figure parts D–F (intravenous CAR-T injection) were each replicated in two independent experiments. In C and D, deaths due to a procedural issue, and not related to disease, are denoted with an X and have not been counted against survival. (B and E) Data are presented as means with error bars representing SEM. (B) P values: *p<0.05, **p<0.01, ***p<0.001, and ****p<0.0001 were determined by two-way ANOVA with Tukey's multiple comparisons test. (E) P values: ***p<0.001 and ****p<0.0001 were determined by multiple unpaired t-tests. ANOVA, analysis of variance; CAR, chimeric antigen receptor; GBM, glioblastoma.

differently in the pons compared with other regions of the brain. Mice treated with $\alpha_v\beta_3$ CAR-T cells were completely protected from lethality as 100% of mice survived long term, whereas 80% of control mice died by day 70 (figure 6C). Importantly, all $\alpha_v\beta_3$ CAR-T cell treated mice remained tumor free for the duration of the experiment. These data show that $\alpha_v\beta_3$ CAR-T cell treatment was highly effective at completely eliminating GBM tumors in vivo without any observable evidence of toxicity or tumor recurrence.

Systemic administration of $\alpha_v\beta_3$ CAR-T cells leads to complete regression of glioblastoma

The previous results demonstrated effective antitumor activity of $\alpha_v\beta_3$ CAR-T cells injected intratumorally. We next aimed to determine if CAR-T cells administered in a systemic manner could migrate to orthotopic GBM tumors. Mice were injected intravenously with 10×10^6 CD19 or $\alpha_v\beta_3$.BB ζ CAR-T cells, and tumor burden was monitored by BLI (figure 6D, online supplemental figure 3B). By day 14, significant tumor regression was evident in mice treated with $\alpha_v\beta_3$.BB ζ CAR-T cells (figure 6D–E). Mice treated with $\alpha_v\beta_3$.BB ζ CAR-T cells remained disease-free for the duration of the experiment and exhibited superior survival compared with mice treated with control CAR-T cells (figure 6F). These results demonstrate that $\alpha_v\beta_3$ CAR-T cells can be administered systemically to effectively treat GBM tumors.

$\alpha_v\beta_3$ CAR-T cells develop long-lived memory following successful GBM treatment

Lastly, we sought to determine whether long-lived memory CAR-T cells develop following eradication of GBM tumors. Both $\alpha_v\beta_3$.28 ζ and $\alpha_v\beta_3$.BB ζ CAR-T cells demonstrated exceptional persistence following tumor clearance as intratumorally administered T cells were easily detectable day 42 post-treatment (figure 7A). A large proportion of $\alpha_v\beta_3$.28 ζ and $\alpha_v\beta_3$.BB ζ CAR-T cells expressed the memory marker CD127 but were also PD-1⁺ (figure 7B,C). Interestingly, mice treated with $\alpha_v\beta_3$.28 ζ CAR-T cells had a significantly higher percentage of CD127⁺ cells compared with mice treated with $\alpha_v\beta_3$.BB ζ CARs.

Some antigen-experienced T cells that exhibit properties of memory and PD-1 expression, yet retain the ability to self-renew in the absence of antigen, are responsive to checkpoint inhibition^{41 42} and express the transcription factor TCF-1. TCF-1 regulates stem-like functions of pre-exhausted T cells (PD-1^{int}), and TCF-1⁺ tumor-infiltrating lymphocytes were shown to be elevated in melanoma patients who had responded to checkpoint receptor inhibition.⁴³ Thus, we sought to determine if $\alpha_v\beta_3$ CAR-T cells express elevated levels of TCF-1 following successful treatment of GBM tumors. We observed that CD8⁺CD127⁺PD-1⁺ populations in $\alpha_v\beta_3$.28 ζ and $\alpha_v\beta_3$.BB ζ CAR-treated mice expressed significantly higher levels of TCF-1 relative to the more terminally differentiated CD127PD-1⁺ populations (figure 7D,E). As expected, TCF-1 expression was not increased in CD8⁺CD127⁺PD-1⁺ cells in mice treated

with CD19 CARs. These data demonstrate that antigen-experienced $\alpha_v\beta_3$ CAR-T cells with self-renewal capacity develop following eradication of tumors.

Finally, persistence of $\alpha_v\beta_3$ CAR-T cells was evaluated 70 days following treatment of GBM tumors. We observed that $\alpha_v\beta_3$ CAR-T cells were still present at day 70 in blood, spleen, and brain (figure 7F). Analysis of memory cell subsets by staining for memory markers CD127 and CCR7 on CAR-T cells was performed. The spectrum of memory T cell differentiation appeared similar in blood, spleen, and brain. Although the highest proportion of CAR-T cells were the more differentiated CCR7CD127⁺ subset, substantial frequencies of CCR7⁺CD127⁺, CCR7⁺CD127⁻, and CCR7CD127⁺ subsets were detected in all tissues in which T cells were recovered (figure 7G). The results of these experiments show that $\alpha_v\beta_3$ CAR-T cells develop memory and persist long term in vivo.

DISCUSSION

We report that CAR-T cells targeting $\alpha_v\beta_3$ represent an attractive candidate for successful therapeutic treatment of malignant and fatal brain tumors. In this study, we determined that $\alpha_v\beta_3$ on the H3K27M mutant diffuse midline glioma, DIPG, and GBM tumors can be targeted by CAR-T cells. Importantly, $\alpha_v\beta_3$ CAR-T cells were highly effective in vivo, mediating significant regression of orthotopic tumors and displaying persistence and memory development. Despite eventual recurrence of DIPG tumors in mice, we were able to rule out specific factors known to be significant limitations of CAR-T cell therapy that typically contribute to relapse: poor CAR expansion, T cell exhaustion, and target antigen escape. Of note, DIPG tumors were large and very well established at the initiation of CAR-T treatment, therefore, a higher dose or repetitive dosing may improve these outcomes. Given the dire prognoses of these high-grade gliomas and absence of effective therapies to treat them, $\alpha_v\beta_3$ CAR-T cell therapy may offer a promising avenue for these patients.

DIPG tumors are notoriously infiltrative.^{38 44} In our orthotopic DIPG experiments, we used a DIPG line that exhibits aggressive growth features (in vitro and in vivo observations), which likely resulted in dissemination and almost certainly contributes to the challenge of achieving successful treatment. Invasion of other areas and niches of the brain by infiltrating DIPG cells occurred as has been demonstrated to happen in human disease and in DIPG mouse xenografts.³³ Despite this, we were able to significantly lower tumor burden, extend progression-free survival, and overall survival through treatment with $\alpha_v\beta_3$ CAR-T cells. Of note is the possible toxicity driven by $\alpha_v\beta_3$ CAR-T cells that use CD28 costimulation in some mice with DIPG tumors. CAR-T cell-induced toxicity was observed in a subset of mice with DIPG following treatment with GD2 CARs containing 4-1BB costimulation.⁴⁵ This study and ours suggests that the anatomical location of DIPG in the pons may be of particular concern, given the critical functions performed there. It is also interesting

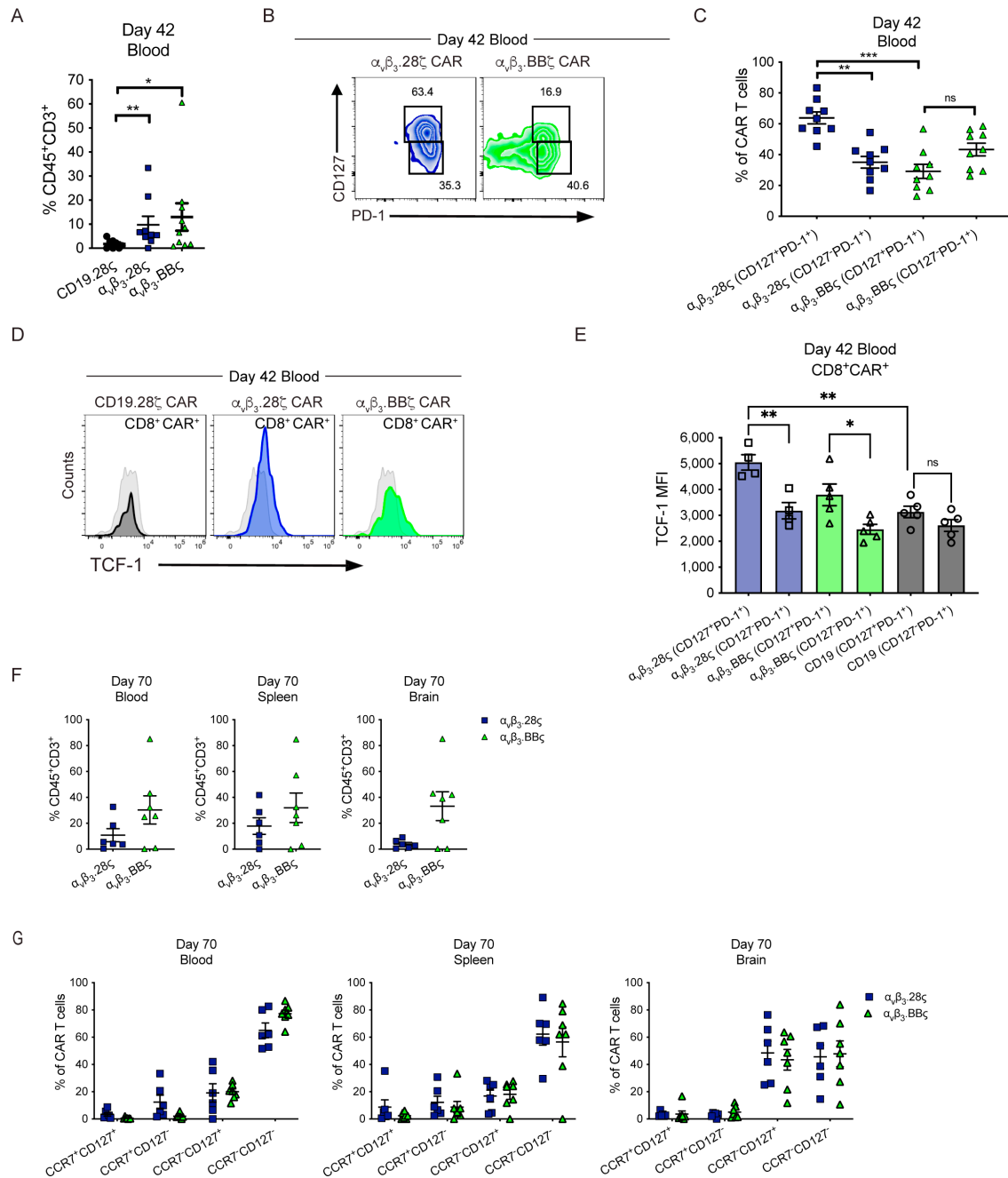


Figure 7 Development of long-lived memory $\alpha_v\beta_3$ CAR-T cells following clearance of GBM tumors in mice. NSG mice implanted orthotopically with 5×10^5 GBM (U87) (eGFP⁺/ffLuc⁺) were treated intratumorally with 2×10^6 CD19.28 ζ CAR, $\alpha_v\beta_3$.28 ζ CAR, or $\alpha_v\beta_3$.BB ζ CAR-T cells on day 21 postimplant. (A) Peripheral blood was collected on day 42 post-treatment for analysis of circulating T cells (CD45⁺CD3⁺) by flow cytometry. (B) Representative flow cytometry dot plots of CD127 and PD-1 expression on CAR⁺ T cells evaluated on day 42 post-treatment. (C) Graphical representation of CD127⁺PD-1⁺ and CD127⁻PD-1⁺ populations in circulating CAR-T cells on day 42 post-treatment. (D) Representative flow cytometry histograms of TCF-1 staining in CD8⁺ CAR-T cells on day 42 post-treatment. Gray-shaded histograms indicate FMO control cells (stained with all fluorochromes minus TCF-1) and black, blue, and green histograms represent CD19.28 ζ , $\alpha_v\beta_3$.28 ζ , and $\alpha_v\beta_3$.BB ζ CAR-T cells, respectively. (E) TCF-1 MFI was calculated in CD127⁺PD-1⁺ and CD127⁻PD-1⁺ populations of CD8⁺ CAR-T cells for individual mice. (F) Peripheral blood, spleen, and brain were harvested on day 70 post-treatment and analyzed by flow cytometry for the presence of human T cells. (G) Memory CAR-T cell populations (CCR7⁺CD127⁺, CCR7⁺CD127⁻, CCR7⁻CD127⁺, and CCR7⁻CD127⁻) were analyzed on day 70 post-treatment in blood, spleen, and brain by gating on CD45⁺CD3⁺CAR⁺ cells. Average CAR⁺ gated event counts (\pm SEM) from all mice were as follows for each harvested tissue: blood: 4692 (\pm 3278); spleen: 13 662 (\pm 4470); brain: 2317 (\pm 1068). (A) P values: * $p < 0.05$ and ** $p < 0.01$ were determined by using an unpaired nonparametric Mann-Whitney test. (C) Significance was determined with a two-way ANOVA with Tukey's multiple comparisons test. (E) P values: * $p < 0.05$ and ** $p < 0.01$ were determined by two-way ANOVA with Tukey's multiple comparisons test. Data are presented as means \pm SEM and symbols in graphs represent individual mice. ANOVA, analysis of variance; CAR, chimeric antigen receptor; GBM, glioblastoma.

to speculate on the role of costimulatory domains in CAR signaling and how these impact toxicities. In the case of orthotopic GBM tumors, we observed complete clearance by $\alpha_v\beta_3$ CAR-T cells without any ensuing tumor recurrence or toxicity. These observations suggest potential differences in the development of treatment-related toxicity based on anatomical location of gliomas and call for incorporation of control or suicide mechanisms for CAR-T cells prior to clinical trials.

Another potential toxicity faced by all new CAR-T cell products in the preclinical phase of development is the risk of so called ‘on-target, off-tumor’ killing of normal cells that may express low-levels of the target antigen. The scFv used in our products does not recognize a murine counterpart. So, while our data suggests highly restrictive $\alpha_v\beta_3$ expression in normal human tissues, the absence of ‘on-target, off-tumor’ killing in our mouse studies does not rule out the possibility of such toxicity in humans. A carefully designed and implemented clinical trial of this product with this potential in mind is therefore warranted.

Others have studied $\alpha_v\beta_3$ targeting CAR-T cells in a limited capacity. Wallstabe *et al.*⁴⁶ suggested that CAR-T cells re-directed against $\alpha_v\beta_3$, were able to control disease in mice engrafted with a single melanoma cell line in limited experiments but did not examine other tumor types or effects on tumor vasculature. In a separate study, $\alpha_v\beta_3$ -expressing melanoma was targeted in a syngeneic mouse model using a CAR-T that incorporated echistatin as the targeting domain, rather than an scFv.⁴⁷ While murine-specific CAR-T was able to slow tumor growth, animals still succumbed to disease. Our study differs from these in three principal ways. First, our $\alpha_v\beta_3$ CAR-T cells use humanized and optimized scFv targeting, which has been shown to decrease the risk of anti-CAR-T cell immune responses as best exemplified by CD19 CARs using a humanized scFv rather than the relapse-prone murine-based FMC63 domain.^{48–49} Second, ours is the first to successfully target the most lethal high-grade gliomas in both children and adults using $\alpha_v\beta_3$ CAR-T cells and extends our earlier work of using CARs to target medulloblastoma.⁵⁰ Third, we demonstrate that intravascular administration of $\alpha_v\beta_3$ CAR-T cells is sufficient to control well-established intracranial GBM in animals.

An unresolved area of interest in the use of CAR-T cells targeting $\alpha_v\beta_3$, is their potential to recognize cells of the tumor vasculature expressing $\alpha_v\beta_3$. A limitation of the xenograft models used here is that anti- $\alpha_v\beta_3$ scFv in the CAR does not bind to murine $\alpha_v\beta_3$. Thus, determining the contribution of tumor-associated endothelial cells being targeted by CAR-T cells is not possible. In the study using echistatin as the targeting domain against $\alpha_v\beta_3$, investigators observed destruction of tumor blood vessels in mice implanted with B16 melanoma, but not resting vessels within normal tissues, and significantly stalled tumor growth.⁴⁷ Future studies are necessary to scrutinize the effects of $\alpha_v\beta_3$ CAR-T cells on tumor vasculature and how this may impact antitumor responses.

Our study demonstrates a renewed potential for targeting integrins, specifically $\alpha_v\beta_3$, for antitumor activity. Importantly, our results demonstrating robust responses in tumor-bearing mice, coupled with the restricted nature of $\alpha_v\beta_3$ expression in normal tissues, underscore the potential for both highly effective and safe use of $\alpha_v\beta_3$ CAR-T cells for treatment of DIPG and GBM in patients. Therefore, results of this study support development of Phase I clinical trials of $\alpha_v\beta_3$ CAR-T cells for adults and children with $\alpha_v\beta_3$ -expressing malignancies.

Acknowledgements We would like to acknowledge the following core facilities at the University of Virginia: The Research Histology Core, the Biorepository and Tissue Research Facility, and the Molecular Imaging Core, which are supported by the University of Virginia School of Medicine and through the University of Virginia Cancer Center National Cancer Institute P30 Center Grant. We would also like to acknowledge the University of Virginia Center for Comparative Medicine for providing animal care and services. The accompanying graphical abstract was created with BioRender.com.

Contributors Conceptualisation: DAC, JdR and DWL. Methodology: DAC, JdR and DWL. Investigation: DAC, JdR, LL and EA. Visualisation: DAC. Funding acquisition: DAC and DWL. Project administration: DWL. Supervision: DAC and DWL. Writing – original draft: DAC. Writing – review and editing: DAC and DWL. Guarantor: DWL.

Funding The Childhood Brain Tumor Foundation (DWL); The V Foundation for Cancer Research (DWL); UVA Strategic Investment Fund (DWL).

Competing interests DWL serves as a consultant to Juno Therapeutics/BMS, Harpoon Therapeutics, and Amgen, and his institution receives clinical trial funding from Kite Pharma/Gilead. His spouse is an employee of Karyopharm Therapeutics. DAC and DWL have a patent application pending based on the results presented in this study. All other authors declare that they have no competing interests.

Patient consent for publication Not applicable.

Ethics approval Human PBMC collection from healthy donors was performed according to an Institutional Review Board approved protocol (UVA-IRB#18842). All animal studies were conducted under a protocol approved by and in compliance with policies set by the Institutional Animal Care and Use Committee.

Provenance and peer review Not commissioned; externally peer reviewed.

Data availability statement Data are available on reasonable request.

Supplemental material This content has been supplied by the author(s). It has not been vetted by BMJ Publishing Group Limited (BMJ) and may not have been peer-reviewed. Any opinions or recommendations discussed are solely those of the author(s) and are not endorsed by BMJ. BMJ disclaims all liability and responsibility arising from any reliance placed on the content. Where the content includes any translated material, BMJ does not warrant the accuracy and reliability of the translations (including but not limited to local regulations, clinical guidelines, terminology, drug names and drug dosages), and is not responsible for any error and/or omissions arising from translation and adaptation or otherwise.

Open access This is an open access article distributed in accordance with the Creative Commons Attribution Non Commercial (CC BY-NC 4.0) license, which permits others to distribute, remix, adapt, build upon this work non-commercially, and license their derivative works on different terms, provided the original work is properly cited, appropriate credit is given, any changes made indicated, and the use is non-commercial. See <http://creativecommons.org/licenses/by-nc/4.0/>.

ORCID iDs

Dustin A Cobb <http://orcid.org/0000-0003-0831-5157>

Daniel W Lee <http://orcid.org/0000-0002-3249-9796>

REFERENCES

- 1 Celgene, ABECMA (idecabtagene vicleuce) [Package Insert] 2021.
- 2 Neelapu SS, Locke FL, Bartlett NL, *et al.* Axicabtagene ciloleuce CAR T-cell therapy in refractory large B-cell lymphoma. *N Engl J Med Overseas Ed* 2017;377:2531–44.
- 3 Abramson JS, Palomba ML, Gordon LI, *et al.* Lisocabtagene maraleuce for patients with relapsed or refractory large B-cell

- lymphomas (TRANSCEND NHL 001): a multicentre seamless design study. *Lancet* 2020;396:839–52.
- 4 Maude SL, Laetsch TW, Buechner J, et al. Tisagenlecleucel in children and young adults with B-cell lymphoblastic leukemia. *N Engl J Med* 2018;378:439–48.
 - 5 Wang M, Munoz J, Goy A, et al. KTE-X19 CAR T-cell therapy in relapsed or refractory mantle-cell lymphoma. *N Engl J Med* 2020;382:1331–42.
 - 6 Munshi NC, Anderson LD, Shah N, et al. Idecabtagene vicleucel in relapsed and refractory multiple myeloma. *N Engl J Med* 2021;384:705–16.
 - 7 Chuntova P, Downey KM, Hegde B, et al. Genetically engineered T-cells for malignant glioma: overcoming the barriers to effective immunotherapy. *Front Immunol* 2018;9:1–19.
 - 8 Rafiq S, Hackett CS, Brentjens RJ. Engineering strategies to overcome the current roadblocks in CAR T cell therapy. *Nat Rev Clin Oncol* 2020;17:147–67.
 - 9 Martinez M, Moon EK. CAR T cells for solid tumors: new strategies for finding, infiltrating, and surviving in the tumor microenvironment. *Front Immunol* 2019;10:1–21.
 - 10 Majzner CMR, Nellan A, Heitzeneder S. Car T cells targeting B7-H3, a pan-cancer antigen, demonstrate potent preclinical activity against pediatric solid tumors and brain tumors. *Clin Cancer Res* 2018;65:S2–3.
 - 11 Du H, Hirabayashi K, Ahn S, et al. Antitumor responses in the absence of toxicity in solid tumors by targeting B7-H3 via chimeric antigen receptor T cells. *Cancer Cell* 2019;35:221–37.
 - 12 Wagner J, Wickman E, DeRenzo C, et al. CAR T cell therapy for solid tumors: bright future or dark reality? *Molecular Therapy* 2020;28:2320–39.
 - 13 Desgrosellier JS, Cheresh DA. Integrins in cancer: biological implications and therapeutic opportunities. *Nat Rev Cancer* 2010;10:9–22.
 - 14 Brooks PC, Clark RA, Cheresh DA. Requirement of vascular integrin alpha v beta 3 for angiogenesis. *Science* 1994;264:569–71.
 - 15 Kumar CC. Integrin alpha v beta 3 as a therapeutic target for blocking tumor-induced angiogenesis. *Curr Drug Targets* 2003;4:123–31.
 - 16 Lim M, Guccione S, Haddix T, et al. $\alpha v \beta 3$ Integrin in central nervous system tumors. *Hum Pathol* 2005;36:665–9.
 - 17 Schnell O, Krebs B, Wagner E, et al. Expression of integrin $\alpha v \beta 3$ in gliomas correlates with tumor grade and is not restricted to tumor vasculature. *Brain Pathol* 2008;18:378–86.
 - 18 Martínez-Vélez N, García-Moure M, Marigil M, et al. The oncolytic virus Delta-24-RGD elicits an antitumor effect in pediatric glioma and DIPG mouse models. *Nat Commun* 2019;10:2235.
 - 19 Wick W, Platten M, Wick A, et al. Current status and future directions of anti-angiogenic therapy for gliomas. *Neuro Oncol* 2016;18:315–28.
 - 20 Gutheil JC, Campbell TN, Pierce PR, et al. Targeted antiangiogenic therapy for cancer using vitaxin: a humanized monoclonal antibody to the integrin $\alpha(v)\beta 3$. *Clin Cancer Res* 2000;6:3056–61.
 - 21 Posey JA, Khzaali MB, DelGrosso A, et al. A pilot trial of Vitaxin, a humanized anti-vitronectin receptor (anti $\alpha v \beta 3$) antibody in patients with metastatic cancer. *Cancer Biother Radiopharm* 2001;16:125–32.
 - 22 Patel SR, Jenkins J, Papadopolous N, et al. Pilot study of vitaxin--an angiogenesis inhibitor--in patients with advanced leiomyosarcomas. *Cancer* 2001;92:1347–8.
 - 23 Hersey P, Sosman J, O'Day S, et al. A randomized phase 2 study of etaracizumab, a monoclonal antibody against integrin $\alpha v \beta 3$, \pm dacarbazine in patients with stage IV metastatic melanoma. *Cancer* 2010;116:1526–34.
 - 24 Brooks PC, Montgomery AM, Rosenfeld M, et al. Integrin $\alpha v \beta 3$ antagonists promote tumor regression by inducing apoptosis of angiogenic blood vessels. *Cell* 1994;79:1157–64.
 - 25 Cooney T, Lane A, Bartels U, et al. Contemporary survival endpoints: an international diffuse intrinsic pontine glioma registry study. *Neuro Oncol* 2017;19:1279–80.
 - 26 Hoffman LM, Veldhuijzen van Zanten SEM, Colditz N, et al. Clinical, radiologic, pathologic, and molecular characteristics of long-term survivors of diffuse intrinsic pontine glioma (DIPG): a collaborative report from the International and European Society for Pediatric Oncology DIPG registries. *JCO* 2018;36:1963–72.
 - 27 Alexander BM, Cloughesy TF. Adult glioblastoma. *JCO* 2017;35:2402–9.
 - 28 Bankhead P, Loughrey MB, Fernández JA, et al. QuPath: open source software for digital pathology image analysis. *Sci Rep* 2017;7:1–7.
 - 29 Liu Z, Wang F, Chen X. Integrin $\alpha v \beta 3$ -targeted cancer therapy. *Drug Dev Res* 2008;69:329–39.
 - 30 Lee DW, Kochenderfer JN, Stetler-stevenson M. T cells expressing CD19 chimeric antigen receptors for acute lymphoblastic leukaemia in children and young adults : a phase 1 dose-escalation trial. *Lancet* 2014;6736:1–12.
 - 31 Shah NN, Lee DW, Yates B. Long-term follow-up of CD19-CAR T-cell therapy in children and young adults with B-ALL. *J Clin Oncol* 2021;20.02262.
 - 32 Busch DH, Fräßle SP, Sommermeyer D, et al. Role of memory T cell subsets for adoptive immunotherapy. *Semin Immunol* 2016;28:28–34.
 - 33 Qin EY, Cooper DD, Abbott KL. Neural precursor-derived pleiotrophin mediates subventricular zone invasion by glioma. *Cell*;170.
 - 34 Venkatesh HS, Tam LT, Woo PJ, et al. Targeting neuronal activity-regulated neuroigin-3 dependency in high-grade glioma. *Nature* 2017;549:533–7.
 - 35 Long AH, Haso WM, Shern JF, et al. 4-1BB costimulation ameliorates T cell exhaustion induced by tonic signaling of chimeric antigen receptors. *Nat Med* 2015;21:581–90.
 - 36 Wherry EJ, Kurachi M. Molecular and cellular insights into T cell exhaustion. *Nat Rev Immunol* 2015;15:486–99.
 - 37 Fuertes Marraco SA, Neubert NJ, Verdeil G, et al. Inhibitory receptors beyond T cell exhaustion. *Front Immunol* 2015;6:1–14.
 - 38 Caretti V, Bugiani M, Freret M, et al. Subventricular spread of diffuse intrinsic pontine glioma. *Acta Neuropathol* 2014;128:605–7.
 - 39 Kawalekar OU, O'Connor RS, Fraietta JA, et al. Distinct signaling of coreceptors regulates specific metabolism pathways and impacts memory development in car T cells. *Immunity* 2016;44:380–90.
 - 40 Salter AI, Ivey RG, Kennedy JJ. Phosphoproteomic analysis of chimeric antigen receptor signaling reveals kinetic and quantitative differences that affect cell function 2019;11.
 - 41 Wieland D, Kemming J, Schuch A, et al. TCF1+ hepatitis C virus-specific CD8+ T cells are maintained after cessation of chronic antigen stimulation. *Nat Commun* 2017;8:1–13.
 - 42 Kratchmarov R, Magun AM, Reiner SL. TCF1 expression marks self-renewing human CD8+ T cells. *Blood Adv* 2018;2:1685–90.
 - 43 Siddiqui I, Schaeuble K, Chennupati V. Intratumoral Tcf1⁺PD-1⁺CD8+ T cells with stem-like properties promote tumor control in response to vaccination and checkpoint blockade immunotherapy. *Immunity* 2019;50:195–211.
 - 44 Kluiver TA, Alieva M, van Vuurden DG, et al. Invaders exposed: understanding and targeting tumor cell invasion in diffuse intrinsic pontine glioma. *Front Oncol* 2020;10:1–13.
 - 45 Mount CW, Majzner RG, Sundaresh S, et al. Potent antitumor efficacy of anti-GD2 CAR T cells in H3-K27M⁺ diffuse midline gliomas. *Nat Med* 2018;24:572–9.
 - 46 Wallstabe L, Mades A, Frenz S, et al. CAR T cells targeting $\alpha v \beta 3$ integrin are effective against advanced cancer in preclinical models. *Adv Cell Gene Ther* 2018;1:e11.
 - 47 Fu X, Rivera A, Tao L, et al. Genetically modified T cells targeting neovasculature efficiently destroy tumor blood vessels, shrink established solid tumors and increase nanoparticle delivery. *Int J Cancer* 2013;133:2483–92.
 - 48 Maus MV, Haas AR, Beatty GL, et al. T cells expressing chimeric antigen receptors can cause anaphylaxis in humans. *Cancer Immunol Res* 2013;1:26–31.
 - 49 Turtle CJ, Hanafi L-A, Berger C, et al. CD19 CAR-T cells of defined CD4+:CD8+ composition in adult B cell ALL patients. *Clin Invest* 2016;126:2123–38.
 - 50 Nellan A, Rota C, Majzner R, et al. Durable regression of medulloblastoma after regional and intravenous delivery of anti-HER2 chimeric antigen receptor T cells. *J Immunother Cancer* 2018;6:30.